NMR Investigations of Self-Diffusion and Shear Thinning for Semidilute Polymer Solutions near the Demixing Transition

B. Manz and P. T. Callaghan*

Department of Physics, Massey University, Palmerston North, New Zealand

Received December 17, 1996; Revised Manuscript Received March 25, 1997[⊗]

ABSTRACT: Pulsed gradient spin echo and rheo-NMR methods are used to investigate semidilute solution properties of high molecular mass polystyrene in cyclohexane, in the vicinity of a demixing transition. The dependence of polymer self-diffusion on temperature and molar mass is measured using PGSE NMR. The molar mass variation is consistent with M^{-2} scaling while the temperature variation in approach to demixing can be modeled as a glass transition process using the WLF equation. The measured values of the demixing transition temperature T_p are consistent with known thermodynamic properties. By using NMR velocimetry, we are able to measure the velocity profiles for the polystyrene solutions when sheared in a cylindrical Couette cell. These profiles, which are consistent with strong shear thinning, are fitted using a power law fluid model, and entanglement renewal times obtained from the power law exponents are consistent with and complementary to tube disengagement times obtained from self-diffusion measurements, this family exhibiting M^3 scaling.

Introduction

A random coil polymer chain in solution experiences a competition between entropic forces which tend to expand the molecule and net attractive forces between the segments which favor collapse. Consequently the average dimension and conformation of a single polymer chain in solution depends upon both solvent and temperature. For an isolated polymer of high molar mass, the temperature at which segment−segment contacts begin to be favored and below which the chain can eventually collapse to form a globule defines the Θ temperature for that polymer and that solvent. For random coil polymers at finite concentration, the reduction of the entropic contribution to the free energy as temperature is decreased leads to a demixing transition, below which the solution will separate into two phases.[1,2] The boundary in temperature (T) and volume fraction (Φ) space represented by this transition is known as the coexistence curve, the extremum of which is known as the critical point. These coil-to-globule and demixing transitions have been the focus of extensive research over many years,[3−10] a particularly well-characterized system being the solution of polystyrene (PS) in cyclohexane (CYH)[11−26] for which the Θ temperature for this system is 34.5 °C[27] and therefore easily accessible.

In this paper we shall be concerned with the demixing transition in the case of semidilute solutions of high molecular weight polymers. A particular feature of such systems is that the dynamics of the polymers is believed to be strongly influenced by the topology arising from entanglement constraints. Any model for polymer motion near the coexistence curve will thus depend on the subtle interplay of thermodynamics and topologically-constrained Brownian motion. Scattering techniques give limited information in this concentration regime due to multiple scattering. In contrast, nuclear magnetic resonance (NMR) provides information about local interactions and dynamics. For example, it is well-known that the translational motion of the polymer can be examined using the pulsed gradient spin echo (PGSE) technique,[28] and such an approach has been used by a number of researcher groups in order to investigate the concentration and molar mass dependence of polymer self-diffusion. There are, however, few reported cases of measurements of temperature dependence of polymer self-diffusion, and we are aware of none relating to demixing. We present here the results of an extensive study of self-diffusion for a range of high molecular weight monodisperse polystyrenes in the solvent cyclohexane, showing how the polymer self-diffusion depends upon concentration, molar mass, and temperature.

Any discussion of the dynamics of entangled polymer will involve the concept of terminal relaxation. In the reptation theory[29,30] this may be identified with the tube disengagement process for which a characteristic time, τ_d, may be defined. In other descriptions the term entanglement formation may apply.[31] It is not the purpose of the present article to address the relative merits of various competing theories, but we will find it convenient to adopt the language of the reptation model and utilize some of the scaling arguments which result from it. However we will investigate the terminal relaxation process using two very complementary NMR methods. In the first approach we shall calculate τ_d from the self-diffusion coefficients obtained via the PGSE NMR method. In the second we shall derive the entanglement renewal time from a measurement of the nonlinear viscosity of the polymer solution. This latter measurement is made possible by our use of NMR velocimetry and, in particular, the determination of shear thinning behavior as exhibited in the velocity profile across the annular gap of a Couette cell. The term "rheo-NMR"[32] has been coined to describe NMR spectroscopy experiments carried out on materials under shear. Our approach to rheo-NMR, focussing as it does on velocity profiling,[33,34] is somewhat novel and, as we shall show, gives us access to the very slow relaxation times associated with the very largest molar mass polymers.

Theoretical Background

The Coexistence Curve. In the Flory−Huggins model, the free energy of mixing at temperature T is given by

[⊗] Abstract published in *Advance ACS Abstracts,* May 1, 1997.

S0024-9297(96)01851-7 CCC: $14.00

$$\Delta G^m = k_B T(N_s + xN_p)\left[\Phi_s \log \Phi_s + \frac{\Phi_p}{x}\log \Phi_p + \chi\Phi_s\Phi_p\right] \quad (1)$$

where Φ_s and Φ_p are respectively the volume fractions of solvent and polymer, k_B is Boltzmann's constant, and χ is the Flory interaction parameter.[1,35] The temperature dependence of χ governs the phase behavior of the polymer solution. For $\chi = {}^1/_2$ the solution is ideal and the polymer chains obey Gaussian statistics, the Θ temperature being where $\chi = {}^1/_2$ for infinitely long polymer chains in a solution with infinitesimal concentration.

Equation 1 leads to a well-known solution for the coexistence curve in (T, Φ_p) space with a critical point (T_c, Φ_c) at its temperature maximum. For temperatures below the demixing transition the attractive intra- and interchain interactions are sufficient to induce a separation into coexisting dilute and more concentrated solution phases. Coexistence curves for PS/CYH solutions were first measured by Shultz and Flory,[36] who found that T_c and Φ_c depend on the chain length χ as

$$\frac{1}{T_c} = \frac{1}{\Theta} + \frac{1}{\Theta\Psi}\left(\frac{1}{\sqrt{x}} + \frac{1}{2x}\right) \quad (2)$$

$$\Phi_c = \frac{1}{1 + \sqrt{x}} \quad (3)$$

where Ψ is known as the entropy parameter.[35] Empirical relationships between T_c, Φ_c, and the molar mass M_w for PS/CYH solutions have been reported by Perzynski *et al.*:[16]

$$\frac{1}{T_c} = \frac{1}{307\ \mathrm{K}}\left(1 + \frac{14.6}{\sqrt{M_w}}\right) \quad (4)$$

$$\Phi_c = 6.8 M_w^{-0.38}\ (\mathrm{g\ cm^{-3}}) \quad (5)$$

The Semidilute Regime and Tube/Reptation Model. The experiments to be described here were performed in the semidilute concentration regime, where polymer chains are entangled with neighboring coils but the segments of chain between entanglements are sufficiently long that their conformation resembles that of an isolated polymer. The semidilute concentration regime exists between concentrations c^* and c^{**}. We shall be concerned with crossover effects associated with the lower boundary given by

$$c^* = \frac{3M_w}{4\pi N_A R_g^3} \quad (6)$$

where R_g is the radius of gyration of the polymer molecules, and N_A is Avogadro's constant. R_g depends on the solvent quality and scales with M_w as

$$Rg \propto Mw^{\nu} \quad (7)$$

where ν is the Flory index and takes a value between 0.5 and 0.6 depending on the degree to which the polymer coil obeys Gaussian or excluded-volume statistics, an effect governed by solvent quality, the Θ solvent corresponding to $\nu = 0.5$.

An empirical relationship for semidilute PS/CYH solutions near the Θ temperature is given by Adam and Delsanti:[14]

$$c^* = 40 M_w^{-0.5}\ (\mathrm{g\ cm^{-3}}) \quad (8)$$

In interpreting the concentration and molar mass dependence of polymer self-diffusion we shall find it convenient to make reference to the tube/reptation model of Doi−Edwards[30,37] and de Gennes.[29,38] The semidilute regime adaptation of that model allows that a unique length scale is incorporated in a depiction of the random coil polymer solution as a melt of blobs. As a result one obtains a scaling of the polymer center-of-mass self-diffusion coefficient D_s with molar mass M_w and concentration Φ as

$$D_s \propto M_w^{-2}\Phi^{(2-\nu)/(1-3\nu)} \quad (9)$$

giving in turn

$$D_s \propto M_w^{-2}\Phi^{-1.75} \quad \text{for a good solvent} \quad (10)$$

$$D_s \propto M_w^{-2}\Phi^{-3.0} \quad \text{for a } \Theta \text{ solvent} \quad (11)$$

In this theory the self-diffusion coefficient of entangled polymers is directly associated with the slowest polymer relaxation process, the tube renewal, and τ_d is the tube disengagement time given by

$$\tau_d = \frac{2R_g^2}{\pi^2 D_s} \quad (12)$$

Nonlinear Viscosity. Polymer melts and solutions exhibit a non-Newtonian dependence of the shear stress on shear rate, commonly known as shear thinning. A number of constitutive equations have been used to describe the relationship between the shear stress, σ_{xy}, and the shear rate, $\dot\gamma = \partial v_x/\partial y$, shown in Figure 1. In one of these, the "power law" fluid, the nonlinear viscosity, $\eta(\dot\gamma)$, can be written as

$$\eta(\dot\gamma) = K\dot\gamma^{n-1} \quad (13)$$

n is known as the power law index and is unity for a Newtonian fluid and less than unity for a shear thinning fluid. The power law constitutive equation is phenomenological and suffers from some defects, for example the divergence of the viscosity at zero shear. However, it provides a useful description in a number of experiments, in particular providing a parameter n which can be used to characterize the degree of shear shinning.

One of the challenges of polymer physics is to find a molecular basis for the constitutive equations. One such is provided by Doi and Edwards, who use the tube disengagement time, τ_d, to parametrize the nonlinear viscosity $\eta(\dot\gamma\tau_d)$.[30,37,39−41] The Curtiss−Bird model,[42−46] also based on a reptation picture for chain dynamics, incorporates the Doi−Edwards result as a special case. In the Curtiss−Bird constitutive equation for the nonlinear viscosity, there exists an adjustable parameter ϵ, known as the link tension coefficient, which may vary between the extremes 0 to 1. The Doi−Edwards case, $\epsilon = 0$, is characterized by a negative power law index in the asymptotic high shear rate limit. Curtiss and Bird find best agreement with experimental data at around $\epsilon = {}^3/_8$ at which n remains positive but small as $\dot\gamma \to \infty$.

A quite different theory for nonlinear viscosity based on the entanglement concept has been developed by Graessley.[31,47] The basic idea in Graessley's theory is that the density of entanglements decreases with increasing shear rate. The onset of shear thinning is

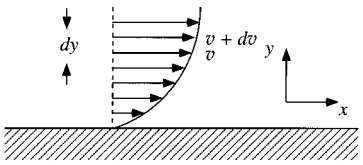

Figure 1. Schematic velocity profile for a fluid flowing along a boundary. The shear rate is defined as $\dot{\gamma} = \partial v_x/\partial y$.

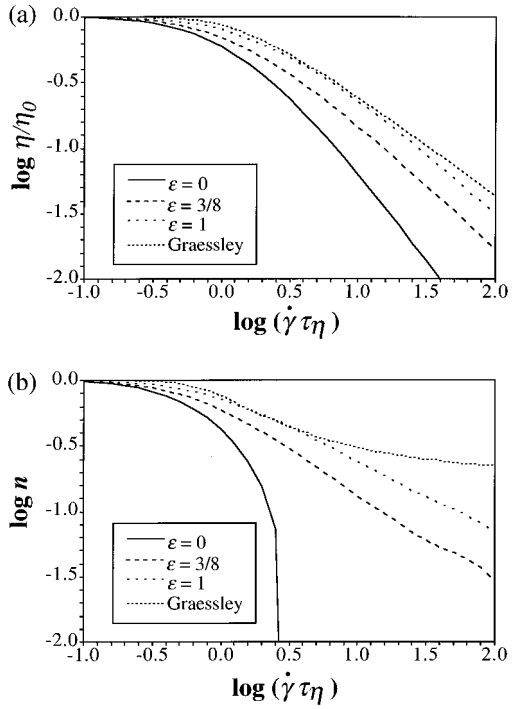

Figure 2. (a) Shear rate dependent viscosities predicted by the Curtiss−Bird and Graessley models. The Doi−Edwards model is incorporated in the Curtiss−Bird model as the special case $\epsilon = 0$. (b) The power law index resulting from the different models in part a. Note that the Doi−Edwards model yields negative values of n for $\log(\gamma\tau_d) > 0.5$.

associated with the shear rate being comparable to the rate of the entanglement formation process τ_η^{-1}, where τ_η is the entanglement formation time and is found to be on the same order as the tube disengagement time τ_d.[48] In the Graessley model, $\eta(\dot{\gamma}\tau_\eta)$ normalized to its value at zero shear viscosity, η_0, is given by a simple closed form expression.

Figure 2a compares the nonlinear viscosity predictions of the Doi−Edwards, Curtiss−Bird, and Graessley models, in which we assume, for convenience, an identity of the tube disengagement time, τ_d, and the entanglement formation time, τ_η. In Figure 2b, we show the resulting dependence of power law index on shear rate.

PGSE NMR and Dynamic NMR Microscopy. Nuclear magnetic resonance imaging utilizes magnetic field gradients to impart a spatial signature to the nuclear spin precession. The local Larmor frequency may be written as $\omega(\mathbf{r}) = \gamma\mathbf{G}\cdot\mathbf{r}$, where $\mathbf{G}$ is the magnetic field gradient, γ the gyromagnetic ratio of the nucleus, and $\mathbf{r}$ the spatial coordinate. The NMR signal is then given by

$$S(\mathbf{k}) = \int \rho(\mathbf{r}) \exp(i2\pi\mathbf{k}\cdot\mathbf{r})\, d\mathbf{r} \qquad (14)$$

where $\rho(\mathbf{r})$ is the nuclear spin density and $\mathbf{k} = (2\pi)^{-1}\gamma\mathbf{G}t$, t being the evolution time of the spins in the presence of the magnetic field gradient. An image of the nuclear

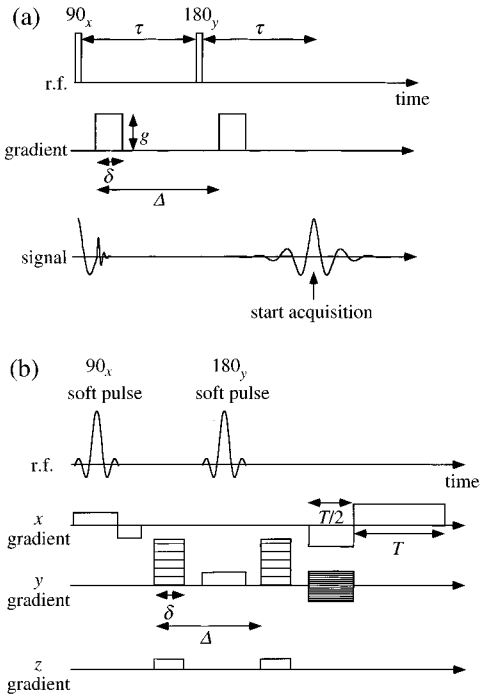

Figure 3. Schematic radio frequency and gradient pulse sequences in which a gradient pulse pair of duration δ and separation Δ is used to phase encode the signal for molecular displacement over the time Δ. (a) The pulsed gradient spin echo pulse sequence is used to measure Brownian motion. (b) The flow imaging pulse sequence incorporates a spatial encoding as well as a displacement encoding.

spin density can be obtained by acquiring $S(\mathbf{k})$ over $\mathbf{k}$-space and subsequent Fourier transformation.

Nuclear displacements can be measured using the pulsed gradient spin echo (PGSE) NMR method. As in the case of position imaging, the method uses magnetic field gradients, but now in "difference mode". Two gradient pulses of duration δ and amplitude g, separated by the delay Δ, are applied in the dephasing and rephasing segments of a spin echo as shown in Figure 3a. Following the spin echo the residual phase shifts arise from displacements $\mathbf{R}$ over the well-defined interval Δ. Under the narrow gradient pulse approximation,[49] the echo signal attenuation is given by

$$E_\Delta(\mathbf{q}) = \int \bar{P}_s(\mathbf{R},\Delta) \exp(i2\pi\mathbf{q}\cdot\mathbf{R})\, d\mathbf{R} \qquad (15)$$

where $\mathbf{q}$ is a reciprocal space vector such that $\mathbf{q} = (2\pi)^{-1}\gamma\delta\mathbf{g}$. $\bar{P}_s(\mathbf{R},\Delta)$ is the ensemble-average displacement propagator, the probability that a spin will displace by $\mathbf{R}$ over the time interval Δ. For Brownian motion, $\bar{P}_s(\mathbf{R},\Delta)$ is Gaussian, and therefore

$$E_\Delta = \exp(-\gamma^2 g^2 \delta^2 D_s \Delta) \qquad (16)$$

For finite gradient pulse durations, Δ is replaced by $\Delta - \delta/3$ and a plot of $\log E_\Delta$ vs $\gamma^2 g^2 \delta^2(\Delta - \delta/3)$ yields a straight line with slope $-D_s$ for simple Brownian motion.[49] The PGSE experiment has been widely used to measure self-diffusion in polymer melts and solutions.[50−57]

In dynamic NMR microscopy the $\mathbf{k}$-space and $\mathbf{q}$-space methods are combined, as shown in the pulse sequence of Figure 3b. $E_\Delta(q)$ is now a contrast in the image, such that

$$S(\mathbf{k},\mathbf{q}) = \int \rho(\mathbf{r}) E_\Delta(\mathbf{q}) \exp(i2\pi\mathbf{k}\cdot\mathbf{r})\, d\mathbf{r} \qquad (17)$$

Table 1. Molecular Weights and Polydispersities of the PS Samples

M_w [g mol−1]	M_w/M_n
330 000	1.04
500 000	1.06
770 000	1.04
1 030 000	1.05
1 450 000	1.06
1 750 000	1.06
3 040 000	1.04
4 000 000	1.06
6 850 000	1.06
9 350 000	1.20
15 000 000	1.25

A double inverse Fourier transformation with respect to **k** and **q** returns the displacement propagator $\bar{P}_s(Z,\Delta)$ for every pixel of the image. In this manner maps of D_s and **v** may be constructed. A detailed description of the method can be found elsewhere.[28]

Experimental Section

Materials. Atactic monodisperse polystyrenes (PS) with different molar masses were purchased from Polymer Laboratories Ltd., Church Stretton, U.K., and used without further purification. The specifications of the samples are shown in Table 1. Spectroscopic grade cyclohexane (CYH) was purchased from Sigma Chemicals Co., St. Louis, MO. The samples for the diffusion experiments were prepared by mixing the appropriate amounts of PS and CYH to make solutions of 5% mass concentration in 2.0 mm o.d. NMR tubes. The tubes were sealed then immediately and kept at a temperature of 60 °C for at least 4 weeks during which time they were occasionally centrifuged back and forth. Convection effects[58] arising from temperature gradients were suppressed by surrounding the polymer sample with a jacket of water.

The samples for the flow experiments could not be sealed for mechanical reasons. The appropriate amounts of PS and CYH to make solutions of 5% mass concentration were mixed in 10.0 mm o.d. NMR tubes and closed with caps. In order to keep solvent evaporation to a minimum, these tubes were then stored in a bottle containing a small amount of CYH and then placed inside a 60 °C water bath for at least 6 weeks, stirring occasionally.

Methods. The polymer self-diffusion coefficients D_s were measured by PGSE NMR as described above using the pulse sequence which is shown in Figure 3a. Measurement of the extremely slow self-diffusion of long-chain polymers (down to $D_s \approx 10^{-14}$ m^2 s^{-1}) requires special techniques.[28] We used a home-built probe with a screened pair of reversed Helmholtz coils as gradient coil. The strength of the magnetic field gradient in this coil may be varied up to 5.0 T m^{-1} with current switching times of less than 1 ms. Because D_s varies by around 4 orders of magnitude between the different samples used, the parameters g, δ, and Δ had to be adjusted appropriately. δ and Δ values ranged from 0.1 to 15 ms and from 10 to 40 ms, respectively. In each diffusion experiment the gradient pulse duration δ was varied in 16 equidistant steps, while the separation Δ and amplitude g were kept constant. A repetition time of 1.5 s was used with up to 256 signal averages, making a total experiment time of up to 1 h 42 min. The temperature was stepped down in 1 °C steps starting at least 15 °C above the phase transition temperature T_p which is different for each sample.

The maximum delay time Δ which could be used in the PGSE pulse sequence was limited by the spin−spin relaxation time T_2 of the polymer. A question arises whether a delay time of $\Delta = 40$ ms is sufficiently long to measure Brownian diffusion for the highest molar masses. In fact, as we shall show, the tube disengagement time τ_d becomes significantly longer than 40 ms for $M_w > 4 \times 10^6$. (Note that for a stimulated echo pulse sequence the maximum delay time Δ is limited not by T_2 but by the spin−lattice relaxation time T_1 which is generally longer than T_2. In practice this means that Δ could be extended by up to an order of magnitude. However, because of the $\tau_d \propto M_w^3$ relationship, this would have the effect of extending the molar mass range by only a factor of 2).

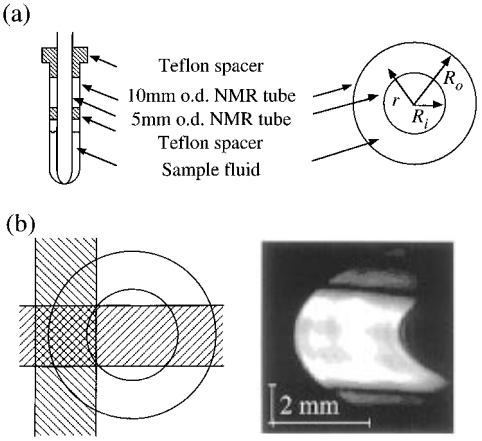

Figure 4. (a) Couette cell used for the rheo-NMR experiments consisting of a 5 mm o.d. NMR tube centered inside a 10 mm o.d. NMR tube. (b) Left hand side: how two orthogonal slices are used to image a small sector of the Couette cell. Right hand side: a proton density image of such a sector. Note that the spatial resolution is set to be greater across the gap and thus leading to the apparent distortion.

Each sample tube prepared for flow imaging was fitted with a 5 mm o.d. NMR tube centered by two Teflon disks, as shown in Figure 4a, a straightforward task with a cylindrical Couette cell. The assembly was then fitted inside the 15 mm rf coil of a standard Bruker 300 MHz NMR probe. A typical sample volume of the Couette cell is 5 mL. The temperature was controlled by a stream of hot air from below.

The inner tube of the cell was rotated at a fixed frequency between 0.5 and 1.0 Hz via a rod connected to a motor sitting on top of the magnet. Due to the rotational symmetry around the inner tube, it is not necessary to record the flow image of the whole sample. A small sector of the sample was imaged instead, as shown in Figure 4b. In order to avoid fold-back in the images, two perpendicular slices had to be selected. Because of the translational symmetry along the axis of the inner tube, no slice selection was needed in this direction, neglecting edge effects. Each image was recorded with a resolution of 4 mm in the x direction and 10 mm in the y direction using 128^2 pixels, two signal averages and 16 q slices with a repetition time of 1 s for each scan, resulting in a total experiment time of 70 min. The temperature was stepped down in steps of 2 °C first, and in 1 °C steps when coming close to the phase transition temperature T_p.

For the Couette geometry an analytical expression for the velocity profile of a power law fluid is available.[34] If the inner cylinder has the radius r_i and spins with the angular velocity ω_0, the angular fluid velocity at radius r is given by

$$v(r) = \omega_0 r \frac{1 - \left(\frac{r}{r_o}\right)^{-2/n}}{1 - \left(\frac{r_i}{r_o}\right)^{-2/n}} \tag{18}$$

r_o is the radius of the outer cylinder. The local shear rate is then given by

$$\dot{\gamma}(r) = r\frac{\partial}{\partial r}\left(\frac{v(r)}{r}\right) \tag{19}$$

or using eq 18

$$\dot{\gamma}(r) = \frac{2\omega_0}{n} \frac{\left(\frac{r}{r_o}\right)^{-2/n}}{1 - \left(\frac{r_i}{r_o}\right)^{-2/n}} \tag{20}$$

Results and Discussion

Variation of D_s with M_w. Figure 5a shows the dependence of D_s on molar mass at different tempera-

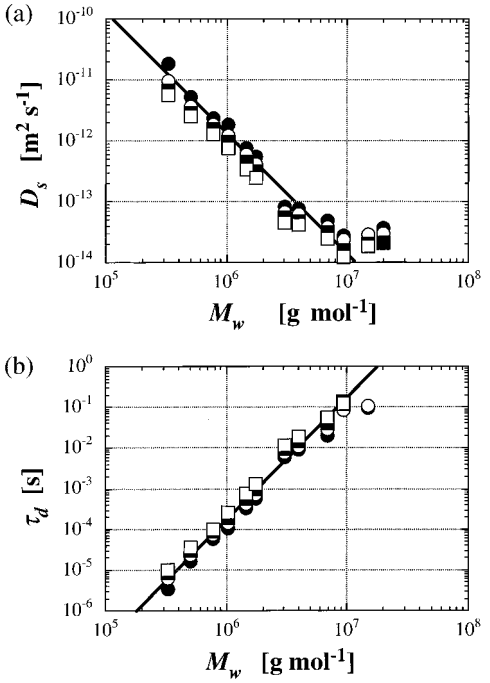

Figure 5. (a) Self-diffusion coefficient D_s shown as function of M_w at $T = 320$ (●), 314 (○), 308 (■), and 305 K (□). For comparison with eq 9, a line with slope −2 is shown as well. (b) Tube renewal time τ_d shown as a function of M_w at different temperatures. The symbols have the same meaning as in part a. For comparison a line with slope 3 is shown as well.

tures. For comparison with the reptation model (and others which predict a similar scaling law) a line corresponding to the $D_s \propto M_w^{-2}$ relationship is shown as well. In the range $5.5 \leq \log M_w \leq 6.5$ this dependence is consistent with the data. The deviation at low molar masses is probably a consequence of crossover. Indeed, from eq 8 it follows that a mass concentration of 5% is below the entanglement concentration c^* for $M_w < 10^6$, and therefore such a transition might be expected at around this molar mass.

The breakdown at upper molar masses is most probably due to the influence of internal polymer segmental motion. Values for the tube disengagement times can be obtained via eq 12 for the data displayed in Figure 5a by using values for R_g from the literature.[9] A graph of τ_d vs M_w so calculated is shown in Figure 5b. For comparison with the reptation model, a line corresponding to the $\tau_d \propto M_w^3$ relationship is shown as well. It is clear that values of τ_d become larger than the echo time of $\Delta = 40$ ms at the highest molar masses used here.

We note in passing that measurements of concentration dependence of D_s were made at a fixed molar mass of 1.75×10^6. No clear scaling was apparent although at concentrations above c^* the data were consistent with $D_s \sim \Phi_p^{-3}$.

Temperature Dependence of D_s. A graph of D_s vs T for different molar masses is shown in Figure 6. $D_s(T)$ decreases monotonically with decreasing temperature. At a particular temperature which depends on M_w, $D_s(T)$ drops sharply. We attribute this effect to demixing and assign the temperature the experimental demixing value T_p. Figure 7 shows a graph of T_p vs M_w along with Perzynski's curve for $T_c(M_w)$ from eq 4. We expect T_p to be equal to T_c only at the molar mass where $\Phi_c = 5\%$ w/w. Using eq 5 this critical molar mass can be found to be 8×10^5 g mol^{-1}. For all other molar masses T_p should be smaller than T_c, a result which is entirely consistent with our data.

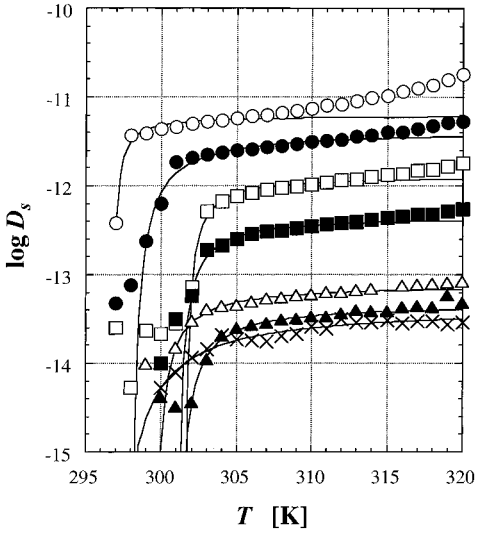

Figure 6. The temperature dependence of D_s near the demixing transition for PS/CYH solutions with a concentration of 5% w/w. The PS molar mass is 330 kD (○), 500 kD (●), 1.03 MD (□), 1.75 MD (■), 3.04 MD (△), 6.85 MD (▲), and 15.0 MD (×), respectively. The lines were obtained using a least-squares fit of eq 25.

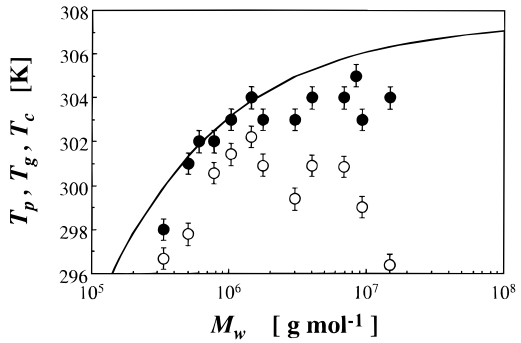

Figure 7. Demixing temperatures T_p (●) and glass transition temperatures T_g (○) as measured by the NMR method plotted vs M_w. Note that T_g is always below T_p. For comparison, the critical temperature T_c from eq 4 is shown (solid line).

We now discuss the temperature dependence, $D_s(T)$. For dilute solutions the temperature dependence of D_s should be given by the Einstein equation[38]

$$D_s(T) = \frac{k_B T}{6\pi\eta_s(T)R_h} \tag{21}$$

where k_B, $\eta_s(T)$ and R_h are Boltzmann's constant, the viscosity of the solvent, and the hydrodynamic radius of the polymer, respectively. This equation does not account for entanglements and cannot explain the temperature dependence of D_s shown in Figure 6. Two different models are suggested. The first is based on fluctuations of the polymer concentration near the critical point, while the second is based on the expected reduction in $D_s(T)$ in the vicinity of a glass transition.

We begin by seeking a simple estimate of the effects of concentration fluctuation on polymer diffusion rate. Let us assume a simple one-dimensional model in which the polymer concentration $\Phi(z)$ fluctuates sinusoidally around a mean value Φ_0 with wavelength λ and amplitude Φ_a:

$$\Phi(z) = \Phi_0 + \Phi_a \cos\left(\frac{2\pi z}{\lambda}\right) \tag{22}$$

Because the Stejskal−Tanner plots are single exponen-

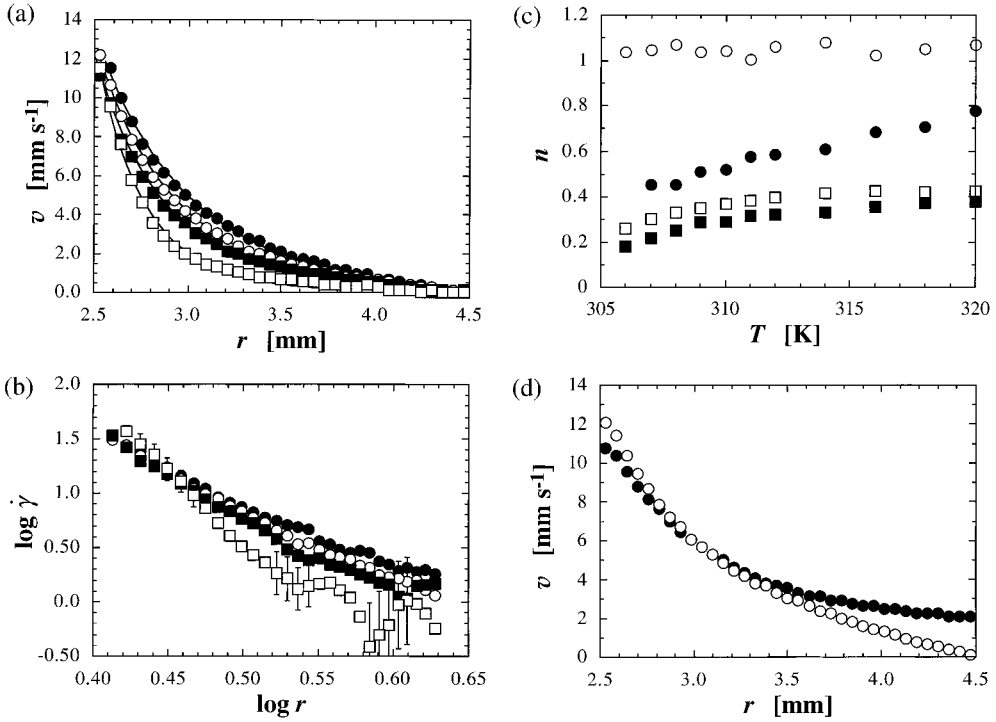

Figure 8. (a) Velocity profiles for the sample with $M_w = 15.0 \times 10^6$ at $T = 314$ (●), 310 (○), 308 (■), and 306 K (□), respectively. The curves fitted to eq 18 are shown as lines. (b) Shear rate obtained from the data shown in part a. Note that a linear relationship is expected from eq 20, if n is constant across the sample. (c) Temperature dependence of the power law index n shown for PS/CYH solutions with $10^{-6}M_w = 1.75$ (○), 6.85 (●), 9.35 (□), and 15.0 (■), respectively. (d) Velocity profiles for the sample with $M_w = 6.85$ g mol^{-1} at $T = 307$ (○) and 306 K (●). Note the slip at the walls at the lower temperature.

tial, the self-diffusion coefficient can be described by an effective constant D_{eff} which is some sort of solution average. This implies that the mean square displacement of the polymer molecules over the time Δ, $\langle z^2 \rangle = D_{eff}\Delta$, must be much larger than the square of the wavelength:

$$\lambda^2 \ll D_{eff}\Delta \tag{23}$$

If we further assume that $D_s \propto \Phi^{-3.0}$ as in a Θ solvent, we obtain

$$D_{eff} = D_0 \frac{1}{1 + \frac{3}{2}\frac{\Phi_a^2}{\Phi_0^2}} \tag{24}$$

where D_0 is the value of D_{eff} for $\Phi_a = 0$.

Φ_a is the only adjustable parameter in eq 24 to be used to describe the temperature dependence of D_{eff}. Because Φ_a must in the range $0 \le \Phi_a \le \Phi_0$, D_{eff} is restricted to values between $^2/_5 D_0 \le D_{eff} \le D_0$. However, close to the demixing transition a sharp decrease of $D_s(T)$ by at least a factor of 5 can be observed, implying that our simple model of concentration fluctuations is not sufficient to explain the experimental results.

We next consider the transition into a glassy state. The temperature dependence of D_s can then be described by the WLF equation[59−61]

$$D_s(T) = D_0 \exp\left(-\frac{B}{T - T_g}\right) \tag{25}$$

where D_0 is the value of D_s far above the glass transition temperature T_g.

The parameters D_0, B, and T_g of eq 25 were fitted to each data set shown in Figure 6 using a least-squares fit. The fit curves are shown as lines in the same figure, while the values of T_g are displayed in Figure 7. It is obvious that the values of T_g are significantly below T_p. A likely reason is that T_p was chosen as the temperature where D_s dropped sharply, while T_g is the temperature where D_s would be zero. In addition, the value of T_g is strongly dependent on the slope of $D_s(T)$ in the demixing regime, and therefore the data points scatter more strongly than T_p.

A question which arises is the following. Given that the glass transition temperature for bulk PS is around 100 °C,[62] what is the reason that T_g for PS in solution approaches the demixing temperature? It is known that for a dilute solution of PS in CYH, T_g is far below the value of T_g for bulk PS[63] and for a PS/CYH solution with a mass concentration of 5%, T_g is still expected to be well below T_c. We suggest that the large concentration fluctuations present when the temperature approaches T_c cause the local value of T_g to exceed the ambient temperature T, thus driving these regions into the glassy state. In such a state the polymer coils will be strongly entangled and may even form long-lived knots,[64] the topology of which is likely to depend on the thermal history of the sample. Samples with different thermal histories may therefore give different experimental self-diffusion results, an effect we have indeed observed.

Velocity Measurements. Figure 8a shows a typical set of velocity profiles at different temperatures. Using eqs 18 and 19 the power law index and local shear rate can be obtained and these are shown in Figure 8b,c. The shear rates obtained from the velocity profiles in Figure 8a are shown in Figure 8b. It is important to note that despite the fact that $\dot{\gamma}$ is not constant across the sample, all data sets show a nearly linear relationship between $\log \dot{\gamma}$ and $\log r$, in accordance with eq 20. The values of the power law index n were obtained from the velocity profiles by using a nonlinear least-squares fit to eq 18. We further remark that the constant value of n across the sample provides a clear indication that shear-

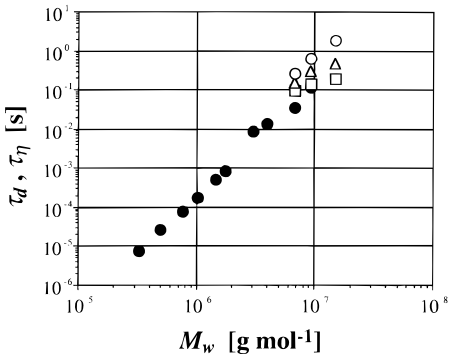

Figure 9. Tube disengagement times τ_d obtained from the diffusion experiments (●) are plotted along with the values of τ_d and τ_η obtained from the velocity profiles using the models of Graessley (○), Curtiss−Bird with $\epsilon = 3/8$ (△), and Curtiss−Bird with $\epsilon = 0$ (□).

induced phase transitions are not apparent at the shear rates employed here.[65,66]

We now turn to the temperature dependence of the power law index displayed in Figure 8c. The sample with $M_w = 1.75 \times 10^6$ exhibits Newtonian behavior at all temperatures and rotation speeds. For all other samples $n(T)$ decreases with decreasing temperature and increasing rotation speed of the inner cylinder. For temperatures below $T = 306$ K, the velocity propagators fluctuate wildly, an effect we attribute to demixing. Near this transition, significant slip is apparent near the inner and outer walls as shown in Figure 8d. Because of the difficulty in obtaining reliable power law indices close to demixing, we have not attempted to fit the temperature dependence using the glass transition model discussed above.

We find no convincing indication that T_p depends on the rotation speed of the inner cylinder. Again, we conclude that there is no evidence for a shear-induced shift of the phase transition temperature in the range of shear rates achievable with our rheometer (up to 100 s^{-1}).

Using both the Curtiss−Bird and Graessley relationships for $n(\dot\gamma\tau_d)$ and $n(\dot\gamma\tau_\eta)$ shown in Figure 2b, we have calculated the relevant relaxation times τ_d and τ_η for data obtained at temperatures well above the demixing transition at T_p. Because the shear rate is not constant across the gap, the question arises as to which value of $\dot\gamma$ determines the rheological behavior of the sample. For simplicity we have chosen the mean shear rate $\dot\gamma_{av}$ which is given by

$$\dot\gamma_{av} = \frac{\int_{r_i}^{r_o} \dot\gamma(r) r \, dr}{\int_{r_i}^{r_o} r \, dr} \tag{26}$$

Using eq 20 this yields

$$\dot\gamma_{av} = \frac{\omega_0}{2n-2} \frac{1}{r^{-2/n} - r_i^{-2/n}} \frac{r_o^{n/(2n-2)} - r_i^{n/(2n-2)}}{r_o^2 - r_i^2} \tag{27}$$

The values of τ_d and τ_η derived from the power law index data corresponding to an inner cylinder rotation speed of 0.75 Hz are plotted vs M_w in Figure 9, for the temperature $T = 310$ K. While we do not show data derived at different inner cylinder rotation speeds, the values of τ_d and τ_η which result are quite consistent with those values shown. Note that the Doi−Edwards limit ($\epsilon = 0$), the Curtiss−Bird optimal value ($\epsilon = {}^3/_8$) and Graessley's model have been used. Also shown are the values for τ_d which were obtained from the diffusion experiments. The τ_d values derived from diffusion measurements and the τ_d and τ_η values obtained from the velocity profiles are remarkably consistent with each other and the entire set is consistent with M_w^3 scaling as expected from the reptation model. Note that the diffusion-derived values of τ_d for $M_w > 4 \times 10^6$, which appear to be below the theoretical values predicted by the reptation model, are in fact unreliable because for these samples τ_d is larger than the PGSE echo time Δ.

We note that the majority of studies of nonlinear viscosity of polystyrene have been carried out under good solvent conditions. However Ballauff *et al.* compare measurements of shear-rate dependent viscosity for 1.77×10^6 g mol^{-1} polystyrene in a Θ solvent, *trans*-decalin, with a good solvent, toluene.[67,68] At high shear rates, the Θ system exhibited some deviation from the constitutive behavior exhibited in Figure 2. This discrepancy they attributed to frictional effects associated with the attractive forces between chains which exist under Θ solvent conditions. However their own data suggest that such effects will be insignificant at the very high molecular weights and relatively low concentrations employed here. In consequence, we see no reason why the constitutive models used in our work on polystyrene in cyclohexane, which have been shown to have some relevance both to melts and to good solvent behavior under entanglement conditions, should not be equally valid in the vicinity of the demixing transition. We would however, expect a complete breakdown under conditions of demixing and coil collapse.

Finally, we emphasise that is not the purpose of this article to compare the relative merits of the Doi−Edwards, Curtiss−Bird, and Graessley theories for nonlinear viscosity. We do show however that all three yield polymer relaxation times which are broadly consistent with tube disengagement times derived from direct NMR measurement of molecular dynamics.

Conclusions

We observe here that the molar mass dependence of self-diffusion for high molecular weight polystyrene in semidilute solution with cylohexane is consistent with the predictions of the tube/reptation model, although we stress again that apparent scaling behavior of the type seen here cannot provide convincing proof. Furthermore the temperature dependence of D_s shows clear manifestations of demixing, and the T_p values obtained are in excellent agreement with the empirical relationship due to Perzynski *et al.* This temperature dependence can be nicely modeled using a simple glass transition picture.

We have demonstrated how two very different NMR methods may be used to evaluate the tube disengagement times for high molar mass polymers. The more traditional method involves the determination of the polymer self-diffusion coefficients by PGSE NMR. For large values of M_w the experiments become very difficult for two reasons. First, large gradients are required in order to encode for the small nuclear spin displacements when the polymers are moving very slowly. Second, the time separating the gradient pulses, Δ, must be longer than the tube disengagement time in order to ensure that Brownian motion determines the dynamics, a condition which is difficult to achieve given that values of Δ are generally limited by the spin-lattice relaxation time (on the order of 500 ms) while the tube disengagement times may well exceed this as the molar mass increases.

The rheo-NMR method provides an appropriate alternative which is well-suited to the highest molar masses. By fitting for the power law index and using various well-known theories for nonlinear viscoelasticity, it is possible to obtain the tube disengagement time (or entanglement formation time) of the polymer. This rheo-NMR method works best at shear rates for which $\dot{\gamma}\tau_\eta > 1$, a condition which can be achieved at quite moderate shear rates for polymers with molar masses in excess of a few million daltons. It is important to note that, in contrast to the PGSE method where the polymer diffusion is measured, the flow imaging method used to obtain the power law index is based on the NMR signal from the solvent and is therefore not limited by the generally short relaxation time of the polymer molecules. The agreement between the terminal relaxation times found by the two methods is therefore all the more remarkable given that one is truly microscopic, based as it is on molecular Brownian motion, while the other gives a macroscopic measure of bulk solution properties.

Acknowledgment. B.M. acknowledges financial support under the "DAAD-Doktorandenstipendien aus Mitteln des zweiten Hochschulsonderprogramms" from the German Academic Exchange Service. The authors are grateful to the New Zealand Foundation for Research, Science, and Technology for major funding. The authors gratefully aknowledge valuable discussions with G. H. Fredrickson, T. C. B. McLeish, S. T. Milner, M. Rubinstein, and E. T. Samulsi, at the NATO ASI on Complex Fluids held in Cambridge, U.K., March 1996.

References and Notes

(1) Flory, P. J. *J. Chem. Phys.* **1942**, *10*, 51.
(2) Huggins, M. L. *J. Phys. Chem.* **1942**, *64*, 1712−1719.
(3) Akcasu, A. Z.; Han, C. C. *Macromolecules* **1979**, *12*, 276−280.
(4) Munch, J.-P.; Hild, G.; Candau, S. *Macromolecules* **1983**, *16*, 71−75.
(5) Park, I. H.; Wang, Q.-W.; Chu, B. *Macromolecules* **1987**, *20*, 1965−1975.
(6) Grosberg, A. Y.; Kuznetsov, D. V. *Macromolecules* **1992**, *25*, 1996−2003.
(7) Yu, J.; Wang, Z.; Chu, B. *Macromolecules* **1992**, *25*, 1618−1620.
(8) Yamakawa, H.; Abe, F.; Einaga, Y. *Macromolecules* **1994**, *27*, 5704−5712.
(9) Arai, T.; Abe, F.; Yoshizaki, T.; Einaga, Y.; Yamakawa, H. *Macromolecules* **1995**, *28*, 5458−5464.
(10) Chu, B.; Ying, Q.; Grosberg, A. Y. *Macromolecules* **1995**, *28*, 180−189.
(11) Adam, M.; Delsanti, M. *J. Phys.* **1983**, *44*, 1185−1193.
(12) Adam, M.; Delsanti, M. *J. Phys. Lett.* **1984**, *45*, L279−L282.
(13) Adam, M.; Delsanti, M. *J. Phys.* **1984**, *45*, 1513−1521.
(14) Adam, M.; Delsanti, M. *Macromolecules* **1985**, *18*, 1760−1770.
(15) Perzynski, R.; Adam, M.; Delsanti, M. *J. Phys.* **1982**, *43*, 129−135.
(16) Perzynski, R.; Delsanti, M.; Adam, M. *J. Phys.* **1987**, *48*, 115−124.
(17) Perzynski, R.; Adam, M.; Delsanti, M. *J. Phys.* **1984**, *45*, 1765−1772.
(18) Nakamura, Y.; Norisuye, T.; Teramoto, A. *Macromolecules* **1991**, *24*, 4904−4908.
(19) Ikier, C.; Klein, H.; Woermann, D. *Macromolecules* **1995**, *28*, 1003−1007.
(20) Fenner, D. B. *J. Chem. Phys.* **1984**, *81*, 5179−5188.
(21) Papazian, L. A. *Polymer* **1969**, *10*, 399−420.
(22) Einaga, Y.; Ohashi, S.; Tong, Z.; Fujita, H. *Macromolecules* **1984**, *17*, 527−534.
(23) Amis, E. J.; Han, C. C.; Matsushita, Y. *Polymer* **1984**, *25*, 650−658.
(24) Nakata, M.; Dobashi, T.; Kuwahara, N.; Kaneko, M. *Phys. Rev. A* **1978**, *18*, 2683−2688.
(25) Scholte, T. G. *J. Polym. Sci. A-2* **1971**, *9*, 1553−1577.
(26) Schmitz, G.; Klein, H.; Woermann, D. *Z. Naturforsch.* **1988**, *43A*, 825−827.
(27) Strazielle, C.; Benoit, H. *Macromolecules* **1975**, *8*, 203−205.
(28) Callaghan, P. T. *Principles of Nuclear Magnetic Resonance Microscopy*; Clarendon Press, Oxford, England, 1991.
(29) de Gennes, P. G. *J. Chem. Phys.* **1971**, *55*, 572−579.
(30) Doi, M.; Edwards, S. F. *J. Chem. Soc. Faraday Trans. 2* **1978**, *74*, 1789−1801.
(31) Graessley, W. W. *Adv. Polym. Sci.* **1974**, *16*.
(32) Nakatani, A. I.; Poliks, M. D.; Samulski, E. T. *Macromolecules* **1990**, *23*, 2686−2692.
(33) Xia, Y.; Callaghan, P. T. *Macromolecules* **1991**, *24*, 4777−4786.
(34) Rofe, C. J.; Lambert, R. K.; Callaghan, P. T. *J. Rheol.* **1994**, *38*, 857−887.
(35) Flory, P. J. *Principles of Polymer Chemistry*; Cornell University Press: Ithaca, NY, 1953.
(36) Shultz, A. R.; Flory, P. J. *J. Am. Chem. Soc.* **1952**, *74*, 4760−4767.
(37) Doi, M.; Edwards, S. F. *The Theory of Polymer Dynamics*; Clarendon Press, Oxford, England, 1986.
(38) de Gennes, P. G. *Scaling Concepts in Polymer Physics*; Cornell University Press, Ithaca, NY, 1979.
(39) Doi, M.; Edwards, S. F. *J. Chem. Soc. Faraday Trans. 2* **1978**, *74*, 1802−1817.
(40) Doi, M.; Edwards, S. F. *J. Chem. Soc. Faraday Trans. 2* **1978**, *74*, 1818−1832.
(41) Doi, M.; Edwards, S. F. *J. Chem. Soc. Faraday Trans. 2* **1978**, *75*, 38−54.
(42) Curtiss, C. F.; Bird, R. B. *J. Chem. Phys.* **1981**, *74*, 2016−2025.
(43) Curtiss, C. F.; Bird, R. B. *J. Chem. Phys.* **1981**, *74*, 2026−2033.
(44) Bird, R. B.; Saab, H. H.; Curtiss, C. F. *J. Phys. Chem.* **1982**, *86*, 1102−1116.
(45) Bird, R. B.; Saab, H. H.; Curtiss, C. F. *J. Chem. Phys.* **1982**, *77*, 4747−4757.
(46) Bird, R. B.; Saab, H. H.; Curtiss, C. F. *J. Chem. Phys.* **1982**, *77*, 4758−4766.
(47) Graessley, W. W. *J. Chem. Phys.* **1967**, *47*, 1942−1953.
(48) Ferry, J. D. *Viscoelastic Properties of Polymers*; John Wiley & Sons: New York, 1980.
(49) Stejskal, E. O.; Tanner, J. E. *J. Chem. Phys.* **1965**, *42*, 288−292.
(50) Fleischer, G.; Zgadzai, O. E.; Skirda, V. D.; Maklakov, A. I. *Colloid Polym. Sci.* **1988**, *266*, 201−207.
(51) von Meerwall, E. D. *Adv. Polym. Sci.* **1983**, *54*, 1−29.
(52) von Meerwall, E.; Amis, E. J.; Ferry, J. D. *Macromolecules* **1985**, *18*, 260−266.
(53) Callaghan, P. T.; Pinder, D. N. *Macromolecules* **1984**, *17*, 431−437.
(54) Callaghan, P. T.; Pinder, D. N. *Macromolecules* **1985**, *18*, 373−379.
(55) Kubo, T.; Nose, T. *Polymer Journal* **1992**, *24*, 1351−1361.
(56) Nose, T. *Annu. Rep. NMR Spectrosc.* **1993**, *27*, 217−253.
(57) Heink, W.; Kärger, J.; Seiffert, G.; Fleischer, G.; Rauchfuss, J. *J. Magn. Reson. A* **1995**, *114*, 101−104.
(58) Manz, B.; Seymour, J. D.; Callaghan, P. T. *J. Magn. Reson. A* (in press).
(59) Edwards, S. F.; Vilgis, T. *Phys. Scr.* **1986**, *T13*, 7−16.
(60) Edwards, S. F. *Polymer* **1994**, *35*, 3827−3830.
(61) Williams, M. L.; Landel, R. F.; Ferry, J. D. *J. Am. Chem. Soc.* **1955**, *77*, 3701−3707.
(62) Brandrup, J.; Immergut, E. H. *Polymer Handbook*; John Wiley & Sons: New York, 1989.
(63) Brown, W.; Stepanek, P. *Macromolecules* **1991**, *24*, 5484−5486.
(64) Brulet, A.; Cotton, J. P.; Lapp, A.; Jannink, G. *J. Phys. II* **1996**, *6*, 331−334.
(65) Rangel-Nafaile, C.; Metzner, A. B.; Wissbrun, K. F. *Macromolecules* **1984**, *17*, 1187−1195.
(66) Debeauvais, F.; Gramain, P.; Leray, J. *J. Polym. Sci. C* **1968**, *16*, 3993−3999.
(67) Ballauff, M.; Krämer, H.; Wolf, B. A. *J. Polym. Sci., Polym. Phys. Ed.* **1983**, *21*, 1205−1216.
(68) Ballauff, M.; Krämer, H.; Wolf, B. A. *J. Polym. Sci., Polym. Phys. Ed.* **1983**, *21*, 1217−1226.

MA961851N